POLITECNICO DI TORINO
Repository ISTITUZIONALE

Estimation of the hydraulic parameters of unsaturated samples by electrical resistivity tomography

Original
Estimation of the hydraulic parameters of unsaturated samples by electrical resistivity tomography / Cosentini, R.M., DELLA VECCHIA, G., Foti, S., Musso, G.. - In: GEOTECHNIQUE. - ISSN 0016-8505. - STAMPA. - 62:7(2012), pp. 583-594. [10.1680/geot.10.P.066]

Availability:
This version is available at: 11583/2440713 since:

Publisher:
Thomas Telford

Published
DOI:10.1680/geot.10.P.066

Terms of use:

This article is made available under terms and conditions as specified in the corresponding bibliographic description in the repository

Publisher copyright

(Article begins on next page)

15 November 2026

Cosentini, R. M. *et al.* (2012). *Géotechnique* **62**, No. 7, 583–594 [http://dx.doi.org/10.1680/geot.10.P.066]

Estimation of the hydraulic parameters of unsaturated samples by electrical resistivity tomography

R. M. COSENTINI*, G. DELLA VECCHIA†, S. FOTI* and G. MUSSO*

In situ and laboratory experiments have shown that electrical resistivity tomography (ERT) is an effective tool to image transient phenomena in soils. However, its application in quantifying soil hydraulic parameters has been limited. In this study, experiments of water inflow in unsaturated soil samples were conducted in an oedometer equipped to perform three-dimensional electrical measurements. Reconstructions of the electrical conductivity at different times confirmed the usefulness of ERT for monitoring the evolution of water content. The tomographic reconstructions were subsequently used in conjunction with a finite-element simulation to infer the water retention curve and the unsaturated hydraulic conductivity. The parameters estimated with ERT agree satisfactorily with those determined using established techniques, hence the proposed approach shows good potential for relatively fast characterisations. Similar experiments could be carried out on site to study the hydraulic behaviour of the entire soil deposit.

KEYWORDS: geophysics; laboratory tests; partial saturation; seepage; suction

Des expériences in situ et en laboratoire ont démontré que la tomographie de résistivité électrique (ERT) est un outil efficace pour l'imagerie de phénomènes transitoires dans les sols. Toutefois, son application pour la quantification de paramètres hydrauliques des sols a été limitée. Dans la présente étude, on effectue des expériences d'arrivée d'eau dans des échantillons de sol non saturés dans un oedomètre équipé pour l'exécution de mesures électriques tridimensionnelles. Des reconstructions de la conductivité électrique effectuées à différents moments ont confirmé l'utilité de l'ERT pour le contrôle de l'évolution de la teneur en eau. On a utilisé, par la suite, des reconstructions tomographiques, conjointement avec une simulation aux éléments finis, afin d'en déduire la courbe de rétention d'eau et la conductivité hydraulique non saturée. Les paramètres estimés avec la tomographie de résistivité électrique s'accordent de façon satisfaisante avec ceux que l'on a déterminé à l'aide de techniques établies ; de ce fait, la méthode proposée présente un bon potentiel pour des caractérisations relativement rapides. Des expériences similaires pourraient être effectuées sur site pour étudier le comportement hydraulique de l'intégralité de la formation de sol.

INTRODUCTION AND BACKGROUND

The water retention curve for a soil can be determined by measuring the water content of samples that are exposed to different values of suction (e.g. Fredlund & Rahardjo, 1993; Masrouri *et al.*, 2008). At each suction increment, the sample must be allowed to reach equilibrium conditions. The time required to reach equilibrium can be significant, as it depends on the hydraulic conductivity of the soil and laboratory equipment (e.g. low air-entry-value porous stones). As a result, establishing the water retention curve for a particular soil can be very time consuming.

A significant reduction in test times can be achieved by determining the water content of a soil sample during unsaturated transient flow events (Kool *et al.*, 1987; Kool & Parker, 1988). This approach relies on the inversion of the boundary value problem, combined with parameter estimation techniques. Outflow or evaporation tests (Romano & Santini, 1999) and infiltration tests (Hopmans & Šimünek, 1999; Young *et al.*, 2002) have been performed in soil columns. Water content is determined from changes in the sample weight as water is expelled from or drawn into the sample as the suction varies. Kool & Parker (1988) suggest that an advantage of this approach is that many combinations of initial and boundary conditions can be used, allowing significant flexibility in the experimental set-up. However, inverse problems may be inherently ill posed, according to the Hadamard definition (Hadamard, 1902), as they may result in non-unique solutions (Tikhonov & Arsenin, 1977).

This study investigates the use of three-dimensional electrical resistivity tomography (ERT) to quantify local changes in water content within a soil sample subject to wetting. The study goes on to explore the feasibility of back-analysis of these results to derive the water retention curve and the unsaturated permeability function of the soil sample. The study relies on the relationship between water content and electrical conductivity: see Mitchell & Soga (2005), Santamarina *et al.* (2001), and the experimental works by Kalinsky & Kelly (1993), Dalla *et al.* (2004) and Attia *et al.* (2008). The inverse problem is solved by minimisation of a suitable objective function, by adopting a grid search approach to avoid local minima. The high number of input points provided by ERT mitigates problems related to the non-uniqueness of the solution. The technique is used to determine the water retention curve for two different soils, which are then compared with results obtained using conventional laboratory techniques.

Manuscript received 22 June 2010; revised manuscript accepted 22 September 2011. Published online ahead of print 22 May 2012.
Discussion on this paper closes on 1 December 2012, for further details see p. ii.

* Department of Structural and Geotechnical Engineering, Politecnico di Torino, Italy.
† Department of Structural and Geotechnical Engineering, Politecnico di Torino, Italy; currently Department of Structural Engineering, Politecnico di Milano, Italy.

EXPERIMENTAL TECHNIQUE AND EQUIPMENT

Electrical measurements in geotechnical laboratory cells have been carried out by placing electrodes on the sidewalls of modified oedometers and Rowe cells to track sedimentation (Blewett *et al.*, 2001) and diffusion (Blewett *et al.*, 2003). Fabric anisotropy has also been investigated by means of electrodes placed at the top and bottom ends of triaxial and oedometer specimens (Kuganenthira *et al.*, 1996), or by

combining distinct sets of vertical and horizontal measurements (McCarter & Desmazes, 1997; McCarter *et al.*, 2005). All of these studies assumed the investigated volume to be electrically homogeneous.

ERT aims to reconstruct the spatial distribution of electrical conductivity: thus the assumption of homogeneity for the investigated volume is not needed. ERT is used to obtain stratigraphic information (e.g. Reynolds, 1997), and has recently been applied in situ to monitor salt and water transport (Zhou *et al.*, 2001; Kemna *et al.*, 2002; Michot *et al.*, 2003; Vanderborght *et al.*, 2005; Battle-Aguilar *et al.*, 2009).

Geotechnical laboratory cells with ERT capabilities have been described by Comina *et al.* (2008), Damasceno *et al.* (2009) and Lee & Santamarina (2010). ERT images have been used to locate heterogeneities (Borsic *et al.*, 2005), to visualise liquefaction (Jinguuji *et al.*, 2007) and to monitor salt diffusion (Comina *et al.*, 2005; Damasceno *et al.*, 2009). In the above-cited works, the use of ERT was limited to providing electrical images, without contributing to quantitative characterisation.

In this study the special oedometer cell described by Comina *et al.* (2008) was used. The device allows the spatial and temporal monitoring of electrical properties under controlled mechanical and hydraulic conditions (Fig. 1). It has an internal diameter of 130 mm, and can accommodate samples of heights of up to 60 mm. The cell has 42 electrodes located on its internal boundary; 16 are equally spaced on the sidewall, and 13 are on each of the base and top plates.

The cell allows drainage by way of the top and base plates. The drainage system is composed of three concentric non-conductive rings with a few micrometres of tolerance between them, resulting in an equivalent permeability of about 6×10^{-6} m/s (Comina *et al.*, 2008). External water pressure and water volume changes are measured by two transducers connected to the bottom drainage line (Fig. 2).

During ERT measurements, electrical current is applied by two electrodes, and other pairs of electrodes measure the induced electrical potential differences. In this study, about 800 measurements were performed for each tomography. The measurement protocol combines 'horizontal' measurements, in which the pairs of electrodes that apply electrical current and those that measure electrical potential are on the sidewall; 'vertical' measurements, in which both types of electrode are on the base and top plates; and 'mixed' measurements, in which the electrodes that apply electrical current are on the sidewall and the measuring electrodes are on the plates.

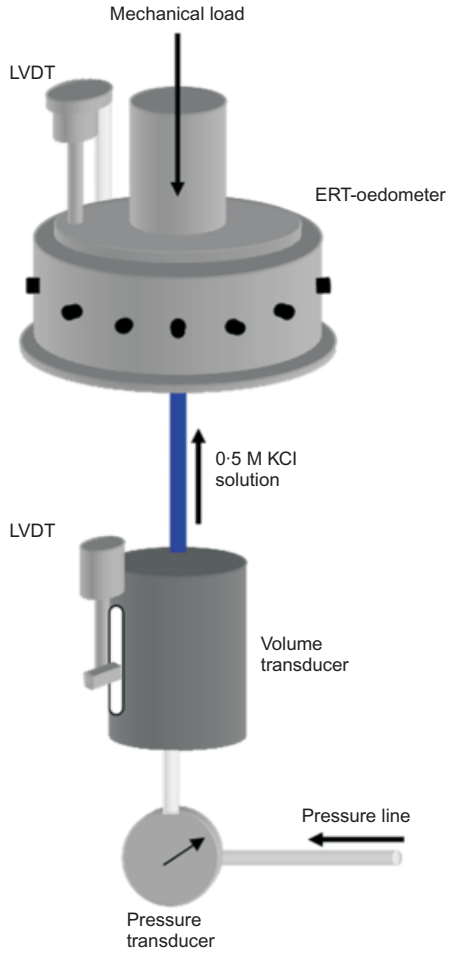


Fig. 2. Experimental assembly (LVDT, linear variable differential transducer)

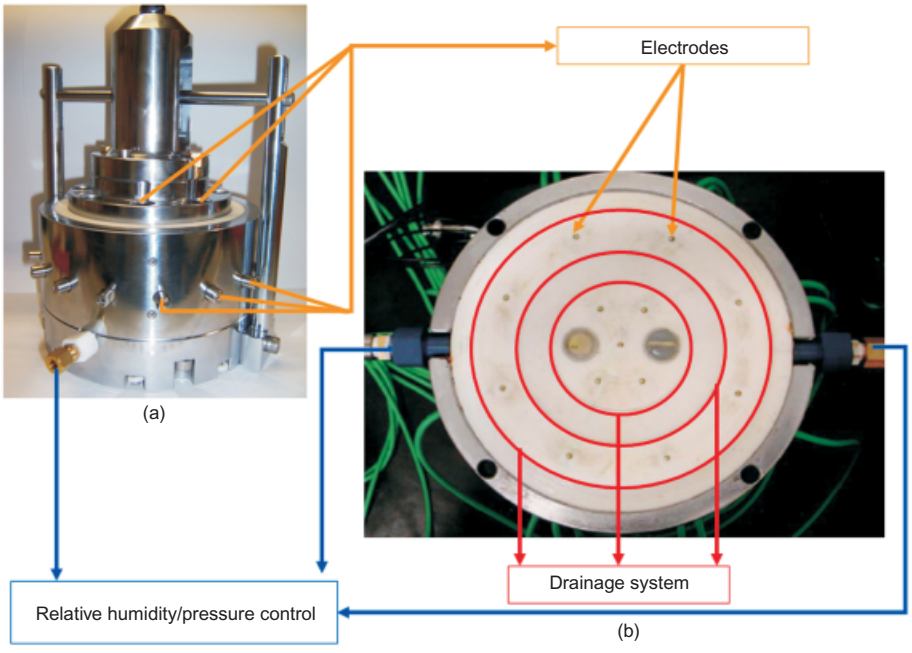


Fig. 1. ERT oedometer cell: (a) overall view; (b) bottom base

The experimental data are then used to reconstruct the electrical conductivity field using a least-squares inversion algorithm with Tikhonov regularisation (Tikhonov & Arsenin, 1977; Borsic *et al.*, 2005). The soil is modelled with a finite-element mesh, and the electrical conductivity of each element, assumed to be isotropic, is estimated.

EXPERIMENTAL INVESTIGATION AND RESULTS

Wetting tests with ERT monitoring were carried out on non-plastic silt and siliceous sand samples collected at the Trecate site in the Ticino River alluvial plain (Northwest Italy). The grain-size distributions of the two materials, prepared by sieving out the gravel fraction, are reported in Fig. 3 and Table 1. In the following discussion, tests performed on the sand are labelled with the letter A, and tests performed on the silt are labelled with the letter B.

Hydraulic and electrical characterisation

The hydraulic and electrical behaviour of the two materials, at the estimated in situ void ratio $e = 0{\cdot}82$ (Godio, 2010, private communication), was first assessed on duplicate specimens prepared by moist tamping. The saturated hydraulic conductivity, measured with a constant head permeameter, is $k_w = 1{\cdot}45 \times 10^{-5}$ m/s for the sand and $k_w = 1{\cdot}85 \times 10^{-6}$ m/s for the silt. Reference water retention curves were determined with a suction-controlled oedometer (Romero *et al.*, 1995) by applying the axis-translation technique. Experimental data obtained upon wetting are reported in Fig. 4. The silt shows a higher air entry value and a lower residual degree of saturation than the sand.

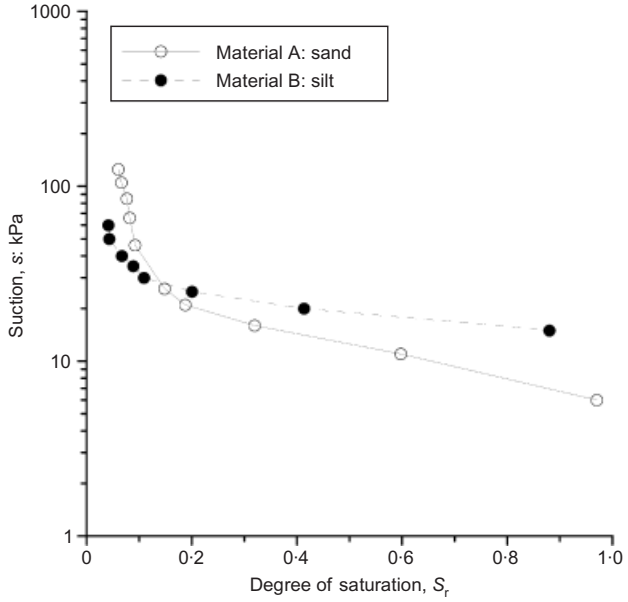


Fig. 4. Water retention curves for the two materials (wetting branch) obtained with the suction-controlled oedometer cell

Electrical characterisation was carried out in the ERT oedometer by measuring the conductivity of homogeneous specimens prepared at different water contents. A 0·5 M KCl (potassium chloride) solution was used to ensure constant water electrical conductivity.

The results were interpreted using Archie's law (Archie,

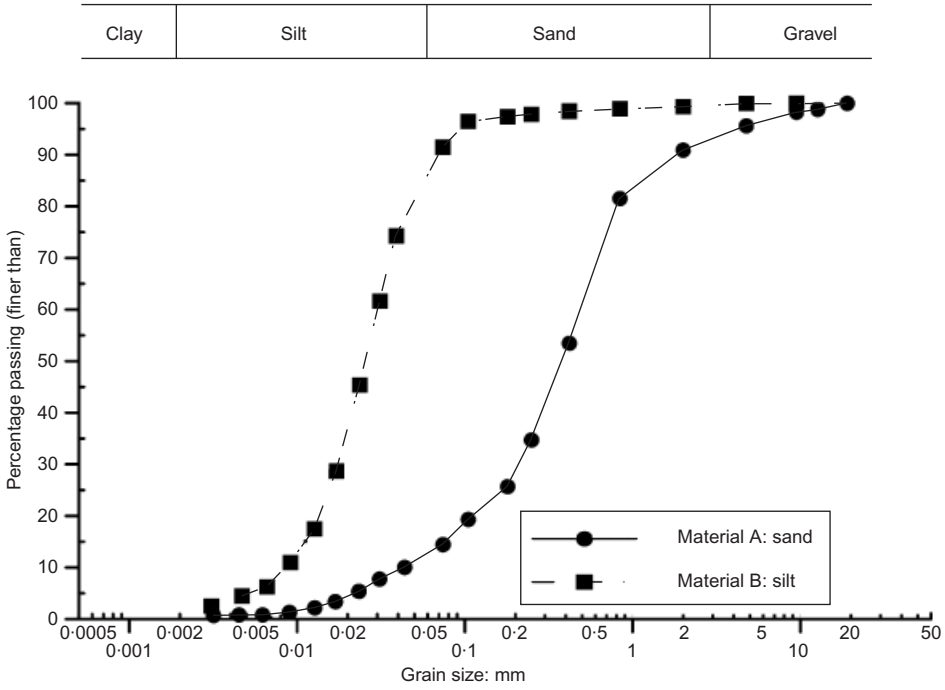


Fig. 3. Grain-size distribution of the sand and silt specimens

Table 1. Particle-size distribution of soils used in this study (MIT classification)

Soil	Sand: %	Silt: %	Clay: %	D_{60}: mm	D_{10}: mm
Trecate sand, A	86·02	13·98	0·0	0·431	0·0378
Trecate silt, B	13·62	86·38	0·0	0·030	0·0085

1942) (Fig. 5), which holds for porous media with non-conductive solid grains

$$\sigma = \sigma_w \phi^p S_r^q \quad (1)$$

where σ and σ_w are respectively the soil and interstitial water electrical conductivities, ϕ is the porosity and p and q are two parameters that take into account the geometry of the interconnected porosity. For constant porosity and water salinity, Archie's law can be written as

$$\frac{\sigma}{\sigma_{sat}} = S_r^q \quad (2)$$

where σ_{sat} is the electrical conductivity of the saturated sample. Values of $q = 2{\cdot}00$ and $q = 1{\cdot}98$ were estimated for the sand and the silt respectively, which agree well with the value originally suggested by Archie (1942).

Experimental protocol

Wetting tests were performed in the ERT oedometer on 4 cm-high specimens, identical to those used for characterisation, at an initial degree of saturation $S_r = 0{\cdot}2$. The specimens were left overnight in the cell to allow the water content to become homogeneous, and were then wetted by applying a water pressure to the drains at the base of the cell. A vertical stress of 2·54 kPa was imposed, and the displacement of the top of the specimen was measured by a linear variable differential transducer (LVDT) to evaluate the volumetric strain (Fig. 2). The porosity variation was less than 1% in all tests, and was thus considered negligible.

Fast (type 1) and slow (type 2) wetting tests were run on both materials. In the type 1 tests, the imposed water pressure was 50 kPa: 90 cm^3 of water were allowed to enter the sand sample in 40 s and 63 cm^3 of water were allowed to enter the silt sample in 50 s (Fig. 6). After closing the bottom drains, all the electrical measurements were performed at a constant global water content for at least 3000 min to assess the local redistribution of water (homogenisation).

The water pressure applied to the bottom drains in the type 2 tests was equal to 5 kPa, inducing a water inflow of 50 cm^3 in 41 min for the sand and 50 cm^3 in 34 min for the silt (Fig. 6). Unlike the type 1 tests, electrical measurements were also performed during wetting to monitor the saturation process. Relevant features of the tests are summarised in Table 2.

Imaging water content changes

Sequences of reconstructed electrical conductivity were analysed to investigate the physical processes occurring within the tested samples.

Figure 7 shows a three-dimensional tomographic reconstruction taken 10 min after drain closure in Test 1A. The image shows all elements within the specimen that, according to ERT, exhibit a conductivity of more than 28 mS/cm.

Figure 8 shows the evolution of electrical conductivity over time in a longitudinal section of the same sample. Time $t = 0$ (Fig. 8(a)) corresponds to the initial condition, consisting of a homogeneous electrical conductivity field. Water inflow took place after the ERT reconstruction shown in Fig. 8(a), and was already completed by the time of occurrence of the ERT reconstructions presented in Figs 8(b), 8(c) and 8(d).

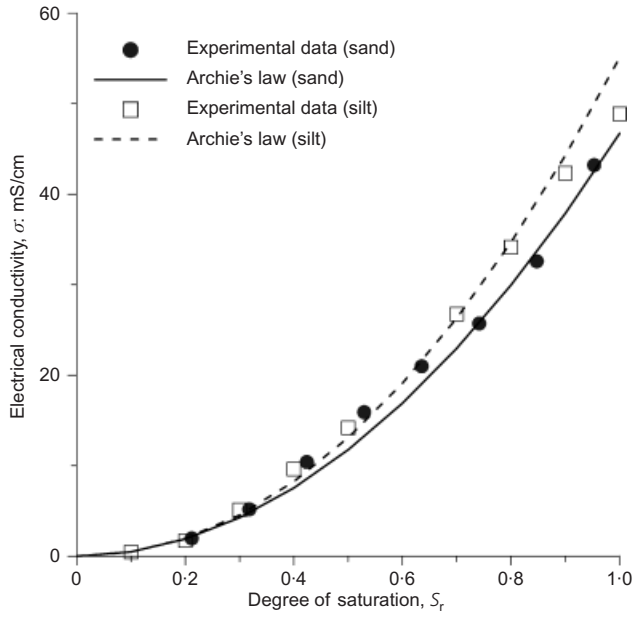


Fig. 5. Relationship between electrical conductivity and degree of saturation for the two materials

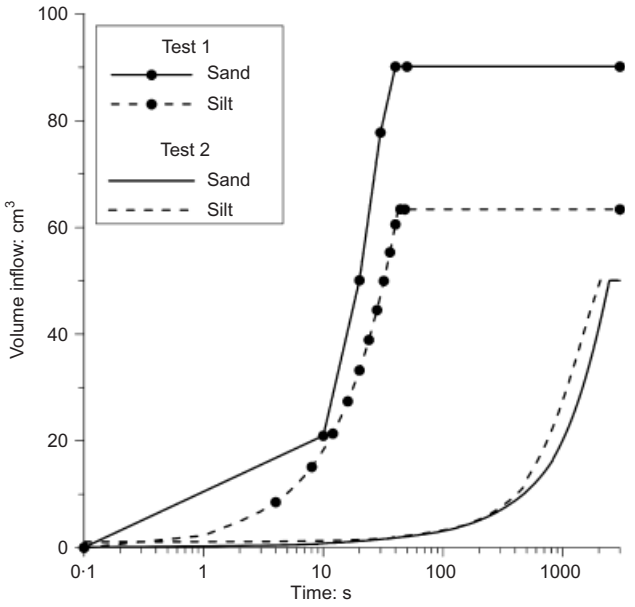


Fig. 6. Time evolution of water inflow for the performed tests

Table 2. Performed inflow tests

Test ID	Material	Imposed external pressure: kPa	Volume inflow: cm^3	Time of flow: min	Total time of ERT monitoring: min
1A	Sand	50	90	0·67	3000
1B	Silt	50	63	0·83	5600
2A	Sand	5	50	41	950
2B	Silt	5	50	34	3300

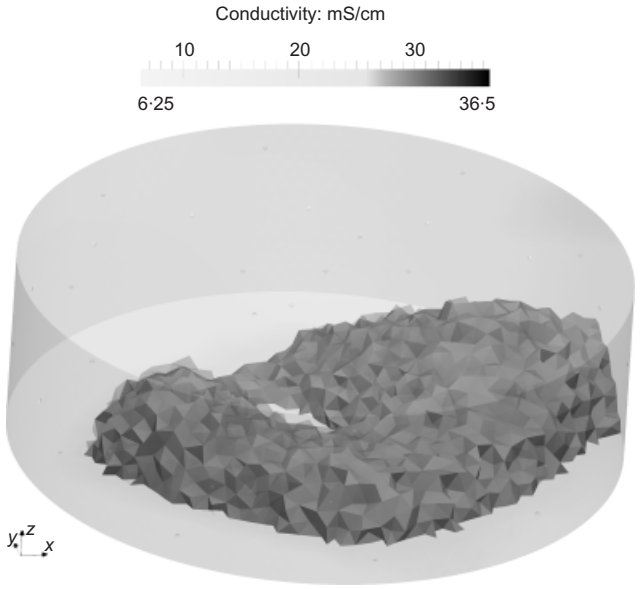


Fig. 7. Test 1A: ERT reconstruction 10 min after drain closure

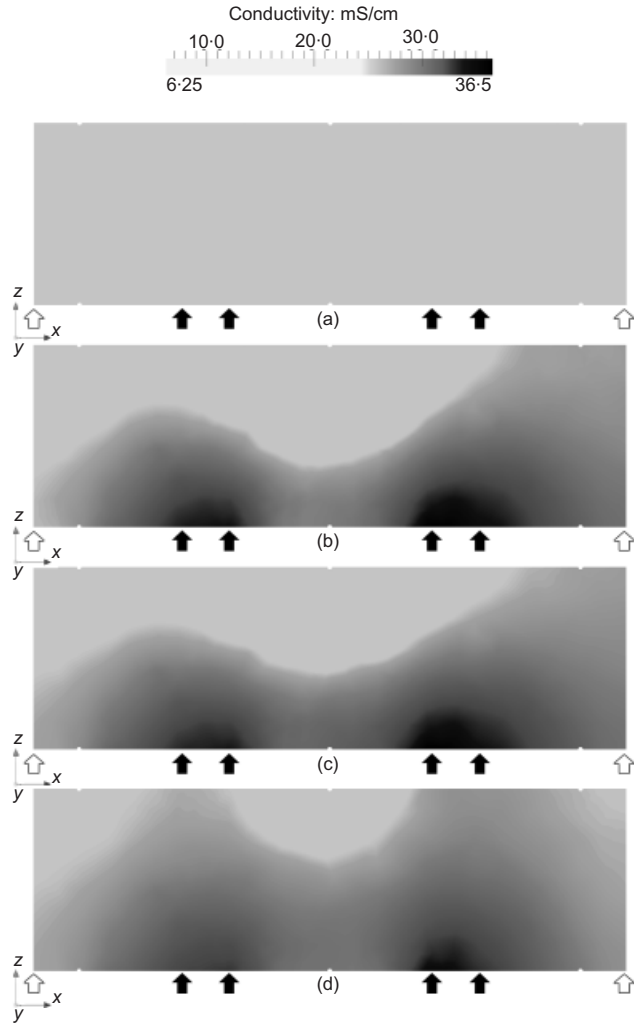


Fig. 8. Test 1A: Time evolution of electrical conductivity over a longitudinal cross-section: (a) $t = 0$ min; (b) $t = 10$ min; (c) $t = 110$ min; (d) $t = 3000$ min (arrows indicate drain positions)

The images in Figs 8(b), 8(c) and 8(d) show various stages after water inflow, and show the redistribution of water at a constant global water content. It is interesting to note that high-conductivity (i.e. high local water content) areas in the sample are initially located in close proximity to the drains, whose position is indicated by arrows in Fig. 8. Over time, the electrical conductivity increases at the top of the sample and decreases near the drains, demonstrating homogenisation.

The variation of electrical conductivity can be linked to water movement due to local pressure gradients: water moves from high water content (low suction) to low water content (high suction) zones. The conductivity distribution at $t = 10$ min (Figs 7 and 8(b)) suggests different efficiencies of the drainage rings. In particular, the flow from the two inner concentric rings (black arrows in Fig. 8) appears to be dominant, as shown by higher conductivity zones during the initial stages of the homogenisation process (Fig. 8).

Figure 9(a) shows changes in electrical conductivity along the axis of symmetry of the sample ($r = 0$ cm). Time $t = 0$ refers to the initial condition, before the wetting stage, and the other times refer to acquisitions performed after wetting had stopped. The progressive increase of electrical conductivity at the top of the specimen is evidence of the migration of water towards this area. Homogenisation continued for 30 h after closure of the drains.

Figure 9(b) shows the electrical conductivity variation along the axis of symmetry for Test 2A. The lines with symbols refer to the inflow stage, the solid line to the time of drain closure, and the dotted lines to the homogenisation process. In Test 2A, the water content appears to increase more homogeneously over time than in Test 1A. This difference can be explained by the lower inflow rate of Test 2A. Indeed, according to Richard's equation (Bear, 1972), low inflow rates are associated with low pressure gradients, that is, with low-water-content gradients.

Similar results were obtained for the silt specimens (Tests 1B and 2B).

ESTIMATION OF THE HYDRAULIC PARAMETERS

Quantitative use of ERT reconstructions has been attempted with different degrees of success in geophysics on the basis of equation (1) (Zhou *et al.*, 2001; Michot *et al.*, 2003; Battle-Aguilar *et al.*, 2009). Some of the above quoted authors have reported mass balance problems, that is, significant differences between the total mass of water (or salt) actually present in the monitored domain and the mass estimated by way of ERT reconstruction. When analysing an in situ infiltration test, Binley *et al.* (2002) found that the increase in the amount of water estimated by the ERT was consistently lower than the real amount, with errors of up to 50%. Singha & Gorelick (2005) found a 50% underestimation error for a synthetic study and a 75 % error for an in situ salt injection test. Indeed, although water content variations are usually well recognised, their quantitative estimation can be affected by large errors. These errors have generally been attributed to poor resolution of the electrical measurements in areas far from the electrodes, and to smoothing introduced in the inversion algorithm (Deiana *et al.*, 2007).

The comparison between the imposed and reconstructed values of water mass in the cell for the experiments discussed above is shown in Fig. 10 in terms of average degrees of saturation. The measured degree of saturation $\overline{S}_r$ was calculated as

$$\overline{S}_r = \frac{V_w}{V_V} \tag{3}$$

where V_w is the volume of water inside the sample and V_V is the volume occupied by the voids. The reconstructed degree of saturation $\overline{S}_r^*$ was evaluated as

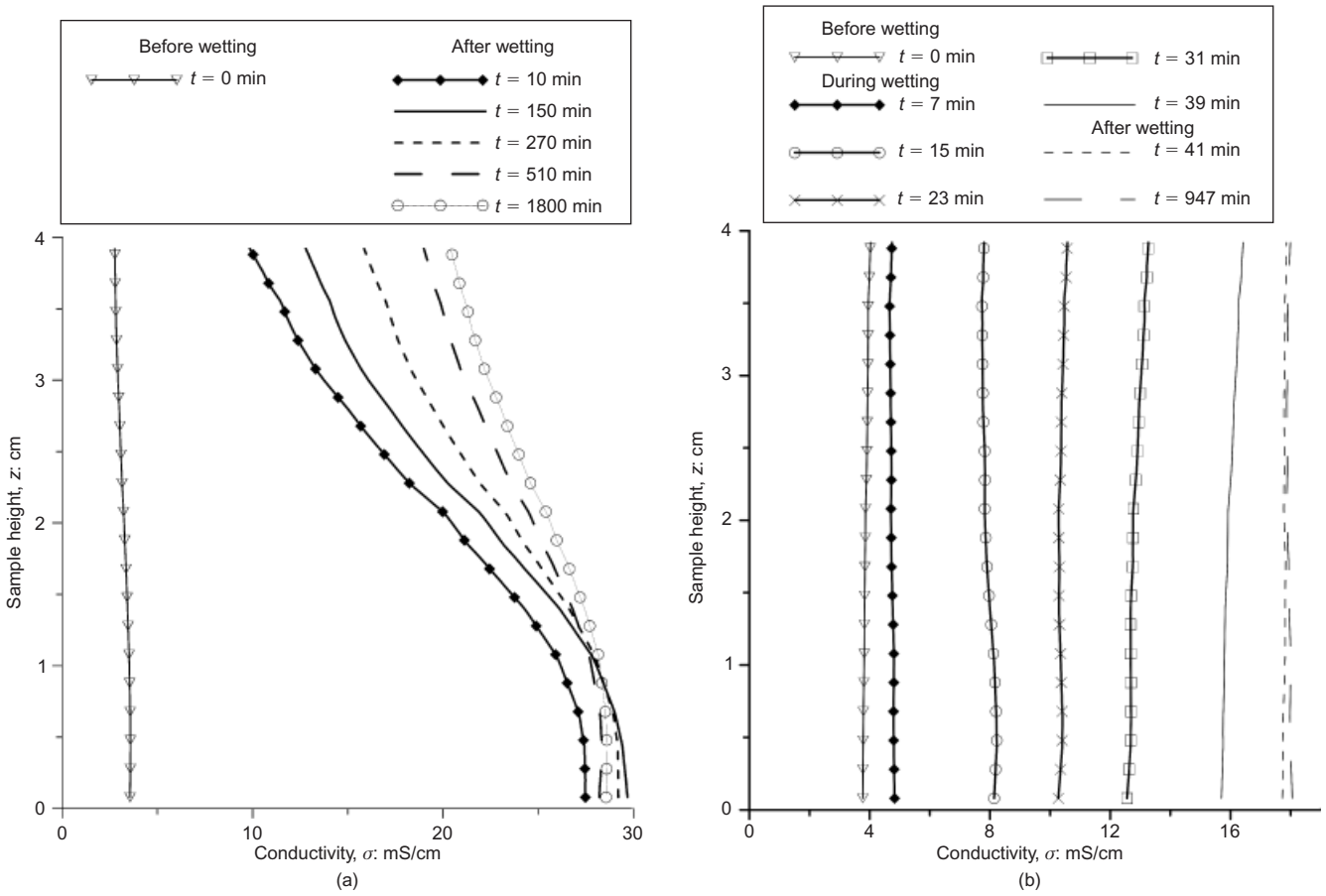


Fig. 9. Conductivity against sample height along axis of symmetry for different times: (a) Test 1A; (b) Test 2A

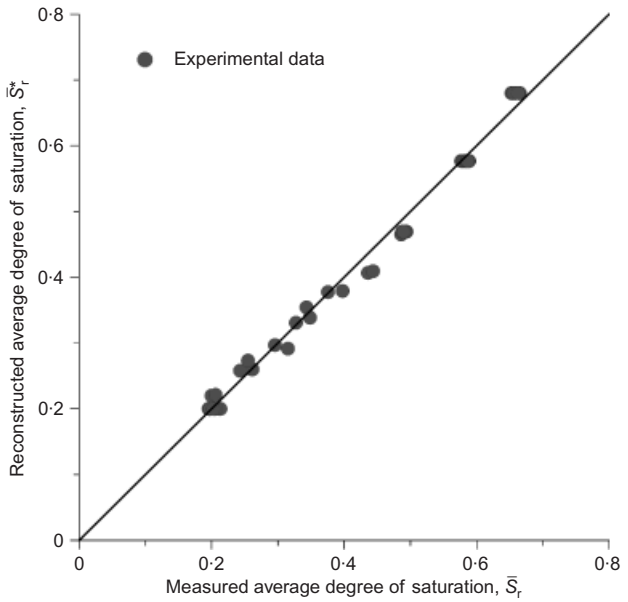


Fig. 10. Imposed and reconstructed average degree of saturation for the entire study dataset

$$\bar{S}_r^* = \left[\frac{\bar{\sigma}^*}{\sigma_{sat}}\right]^{1/q}, \tag{4}$$

where $\bar{\sigma}^*$ is the spatial average of the reconstructed electrical conductivity.

Thanks to the presence of electrodes on all the boundaries of the cell, and to the large number of measurements, water content changes were correctly detected: that is, no mass-balance inconsistency was recorded. This is a fundamental prerequisite for the quantitative interpretation of the results and the parameter estimation procedure adopted in this work.

Formulation of the direct problem: numerical simulation of the physical process

The experimentally derived spatial distribution of the electrical conductivity at different times was compared with the results of a numerical simulation. The physical process was modelled with the continuity equations of water and air, which were numerically integrated using the finite-element method. A back-analysis aimed at identifying the water retention curve and the relative permeability function was then performed. The adopted sequential approach can be referred to as 'uncoupled hydro-geophysical inversion' (Hillel *et al.*, 2010).

Mass balance for water and air was imposed through the partial differential equations

$$\begin{aligned} \frac{\partial(\phi S_r \rho_w)}{\partial t} + \nabla \cdot (\rho_w \boldsymbol{q}_w) &= 0 \\ \frac{\partial[\phi(1-S_r)\rho_a]}{\partial t} + \nabla \cdot (\rho_a \boldsymbol{q}_a) &= 0 \end{aligned} \tag{5}$$

where ρ_i and u_i are the density and the pressure of the ith phase, $\boldsymbol{q}_i$ is the specific discharge and ϕ is the porosity.

Darcy-like laws were used to model the flow of both water and air

$$\boldsymbol{q}_{\mathrm{w}} = -\boldsymbol{k}_{\mathrm{w}}(S_{\mathrm{r}})\nabla\left(z + \frac{u_{\mathrm{w}}}{\rho_{\mathrm{w}} g}\right)$$
$$\boldsymbol{q}_{\mathrm{a}} = -\boldsymbol{k}_{\mathrm{a}}(S_{\mathrm{r}})\nabla\left(z + \frac{u_{\mathrm{a}}}{\rho_{\mathrm{a}} g}\right) \quad (6)$$

where $\boldsymbol{k}_{\mathrm{a}}$ and $\boldsymbol{k}_{\mathrm{w}}$ are functions of the degree of saturation. The unsaturated hydraulic conductivity k_{w} was assumed to be isotropic, and dependent on the degree of saturation S_{r} through the power law (Brooks & Corey, 1964)

$$k_{\mathrm{w}} = k_{\mathrm{w}}^{\mathrm{sat}} k_{\mathrm{w}}^{\mathrm{rel}} = k_{\mathrm{w}}^{\mathrm{sat}} S_{\mathrm{r}}^{\beta} \quad (7)$$

where $k_{\mathrm{w}}^{\mathrm{sat}}$ is the saturated water conductivity, $k_{\mathrm{w}}^{\mathrm{rel}}$ is the relative permeability function and β is an experimental parameter. The following relationship by Corey (1954) was used for the air conductivity

$$k_{\mathrm{a}} = k_{\mathrm{a}}^{\mathrm{dry}}\left(1 - S_{\mathrm{r}}^2\right)\left(1 - S_{\mathrm{r}}\right)^2 \quad (8)$$

where $k_{\mathrm{a}}^{\mathrm{dry}}$ is the conductivity value in dry conditions.

The water retention curve was modelled with the van Genuchten relationship (van Genuchten, 1980)

$$S_{\mathrm{e}} = \frac{S_{\mathrm{r}} - S_{\mathrm{r}}^{\mathrm{RES}}}{1 - S_{\mathrm{r}}^{\mathrm{RES}}} = \left[\frac{1}{1 + (\alpha s)^n}\right]^m \quad (9)$$

where S_{e} is the effective degree of saturation, $S_{\mathrm{r}}^{\mathrm{RES}}$ is the residual degree of saturation, α, n, m are experimental parameters, and $s = u_{\mathrm{a}} - u_{\mathrm{w}}$ is the matric suction. Hysteresis of the retention curve was neglected, because the experiments involved mainly wetting processes.

Finally, the constitutive laws for the two fluids were expressed as

$$\rho_{\mathrm{w}} = \rho_{\mathrm{w0}} \exp\left(B_{\mathrm{w}} u_{\mathrm{w}}\right)$$
$$\rho_{\mathrm{a}} = \frac{m_{\mathrm{a}} u_{\mathrm{a}}}{RT} \quad (10)$$

where ρ_{w0} is the density of water at atmospheric pressure, B_{w} is the bulk compressibility of water, m_{a} is the mass fraction of air considered as an ideal gas, R is the ideal gas constant and T is the absolute temperature. The following values were assumed: $\rho_{\mathrm{w0}} = 1000\ \mathrm{kg/m^3}$; $B_{\mathrm{w}} = 1 \times 10^{-6}\ \mathrm{kPa^1}$; $m_{\mathrm{a}} = 28{\cdot}96\ \mathrm{kg/mol}$; $R = 8{\cdot}31432\ \mathrm{J/(mol\,K)}$ and $T = 298{\cdot}23\ \mathrm{K}$.

Equations (5), with appropriate initial and boundary conditions, represent the direct problem, which was solved with commercial software (Comsol Multiphysics) in terms of pore water and air pressures.

To optimise computational costs, the tests were treated as axis-symmetric. The domain was discretised with a mesh composed of three-node triangular elements. The mesh was refined near the drains.

The boundary of the specimen was assumed to be impermeable to water and air, except for the drains, where the experimentally measured flux of water was imposed during the inflow stage. The initial value of water pressure was determined through the retention curve (Equation (9)), setting the degree of saturation as $S_{\mathrm{r}} = 0{\cdot}2$.

The finite-element solution of the direct problem is given in terms of the nodal variables u_{a} and u_{w}. The degree of saturation and the electrical conductivity were predicted through the retention curve (equation (9)) and Archie's law (equation (2)).

Formulation of the inverse problem

The inverse problem was formulated as a non-linear optimisation process in which α, n, m and β (the three van Genuchten parameters and the relative permeability exponent respectively) can be estimated by minimising a suitable objective function. The objective function expresses the discrepancy between the observed and predicted system responses. The nodal values of the electrical conductivity (predictions) were compared with the corresponding ERT-reconstructed values (observations), with the latter averaged along 30 different longitudinal sections. The averaging procedure smooths local inhomogeneities and anomalies; this makes the axis-symmetric numerical solution and the three-dimensional tomographic reconstruction comparable.

Following Menke (1989), the prediction error, or misfit, $\boldsymbol{e}$ was defined as

$$\boldsymbol{e} = \boldsymbol{\sigma} - \boldsymbol{\sigma}^* \quad (11)$$

In the above, $\boldsymbol{\sigma}$ and $\boldsymbol{\sigma}^*$ are vectors which contain the nodal simulated values $\sigma(\boldsymbol{x}, t)$ and the corresponding ERT values $\boldsymbol{\sigma}^*(\boldsymbol{x}, t)$ for each node and monitoring time t.

The objective function is a measure of the error length. Here, the L1 norm of the misfit was chosen as objective function

$$\|\boldsymbol{e}\|_1 = \sum_{j=1}^{N} |e_j| = \sum_{j=1}^{N} \left|\sigma_j - \sigma_j^*\right| \quad (12)$$

where N is the product of the number of nodes in the finite-element mesh and the number of monitoring times. Neglecting the influence of the error covariance matrix (and therefore neglecting the influence of the geometrical distribution of electrodes and of the measurement sequence on the precision and independence of reconstructed values), parameter estimates are thus obtained by minimising $\|\boldsymbol{e}\|_1$.

Parameter sensitivity analysis

In previous works the estimation of water retention parameters was achieved by minimising objective functions based on a limited number of points. For instance, Young *et al.* (2002) characterised the hydraulic behaviour of unsaturated samples during wetting in vertical columns using the cumulative flux of water and the measurements performed by two tensiometers at different heights.

The points where the input data for the inverse problem are collected strongly influence the accuracy of parameter estimation (Kool & Parker, 1988). Accuracy is higher if these points are located where the variables used in the inverse analysis have a strong dependence on the hydraulic parameters.

ERT has the advantage of providing a large number of sampling points, since tomography simultaneously reconstructs the spatial distribution of the electrical conductivity within the specimen. Nevertheless, it is important to make sure that, during the test, such distribution is sensitive to the hydraulic parameters.

To check the sensitivity of the electrical conductivity to the parameters of both the van Genuchten and relative permeability relationships, a synthetic type 1 test was simulated modelling the behaviour of an ideal sample, supposed to have a defined set of parameters ($\alpha = 1{\cdot}12 \times 10^{-1}\ \mathrm{kPa^{-1}}$, $n = 3{\cdot}5$, $m = 0{\cdot}71$ and $\beta = 6$). These settings were employed to generate a vector $\boldsymbol{\sigma}_{\mathrm{ref}}(t)$ that was used as the synthetic reference.

A parametric study was then performed by varying one single parameter while keeping the others fixed. The results shown in Fig. 11 are interpreted at different time steps in terms of the evolution of the normalised difference

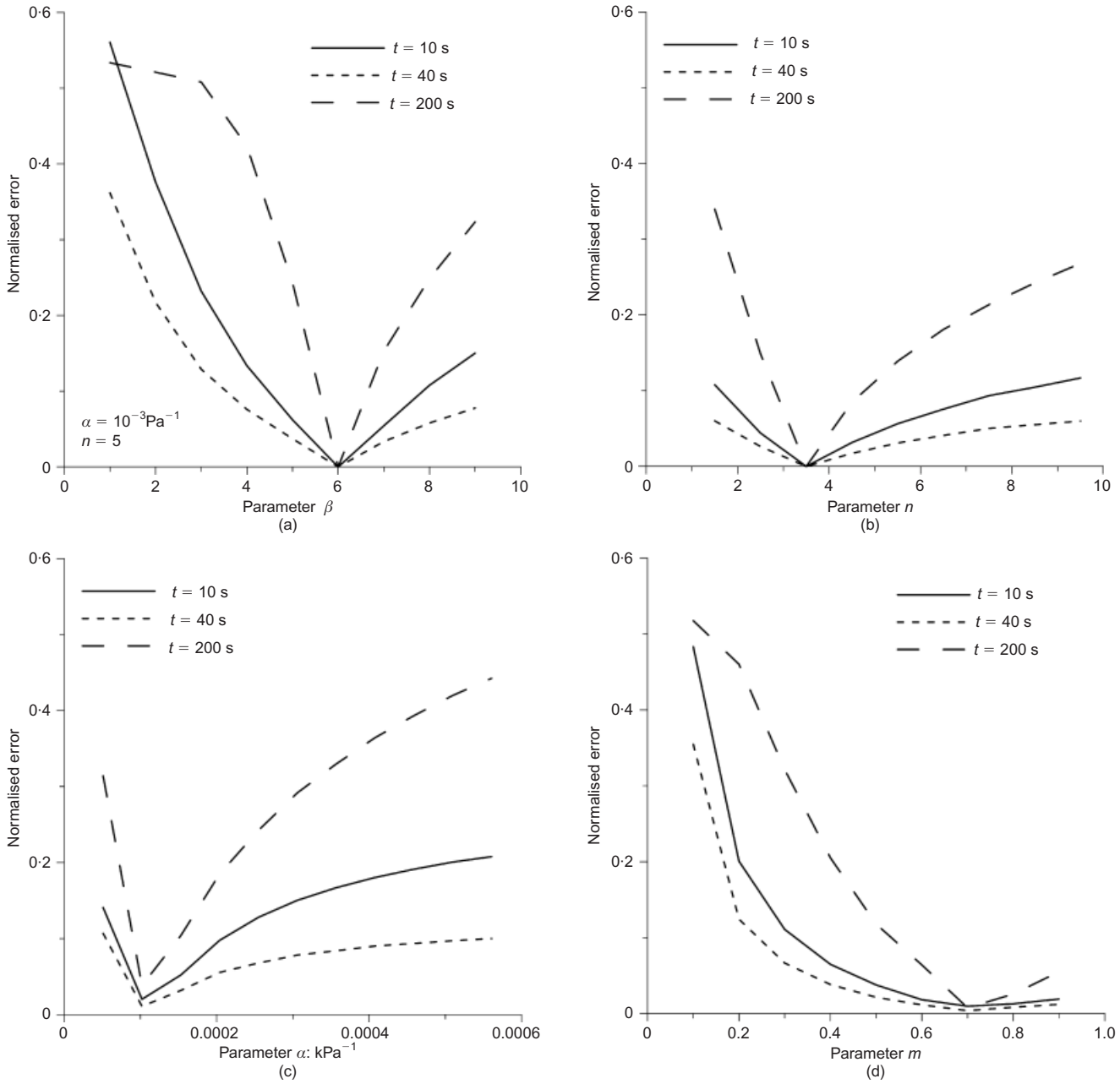


Fig. 11. Parametric analysis of influence of model parameters: (a) β; (b) n; (c) α; (d) m

$$\mathrm{err}_1(\tau) = \frac{\|\boldsymbol{\sigma}(\tau) - \boldsymbol{\sigma}_{\mathrm{ref}}(\tau)\|_1}{\|\boldsymbol{\sigma}_{\mathrm{ref}}(\tau)\|_1}, \tag{13}$$

where τ is a dummy time variable.

Figure 11(d) shows that the solution of the problem is insensitive to m for values of m greater than 0·5. In light of this, the number of unknowns was reduced by introducing the relationship proposed by van Genuchten (1980)

$$m = 1 - \frac{1}{n} \tag{14}$$

A preliminary study on parameter sensitivity plays a crucial role in choosing the time steps of the tomographic acquisitions. As an example, the solution for $t = 40$ s exhibits a lower sensitivity to the parameters than that for $t = 10$ s or $t = 200$ s (Fig. 11). Time choice also depends on the specific parameter to be estimated: for example, according to Fig. 11(a), when $t = 200$ s, varying β from 1 to 3 does not significantly affect the solution.

Solution of the inverse problem and results

The inverse problem was solved with a systematic exploration of the model parameter space. The objective function $\|\boldsymbol{e}\|_1$ (sum of the errors in the L1 norm) was evaluated on a regular grid of values for α, n and β. The range of variation of each parameter was established on the basis of the soil type (see Table 3).

The explored model parameter space, in terms of water retention curve and relative permeability function, is reported in Fig. 12. The boundaries of this space (solid lines)

Table 3. Boundary values for unknown hydraulic parameters in inversion process

Parameter	Maximum value	Minimum value
α: kPa^{-1}	1	1×10^{-3}
β	6	2
n	5	2

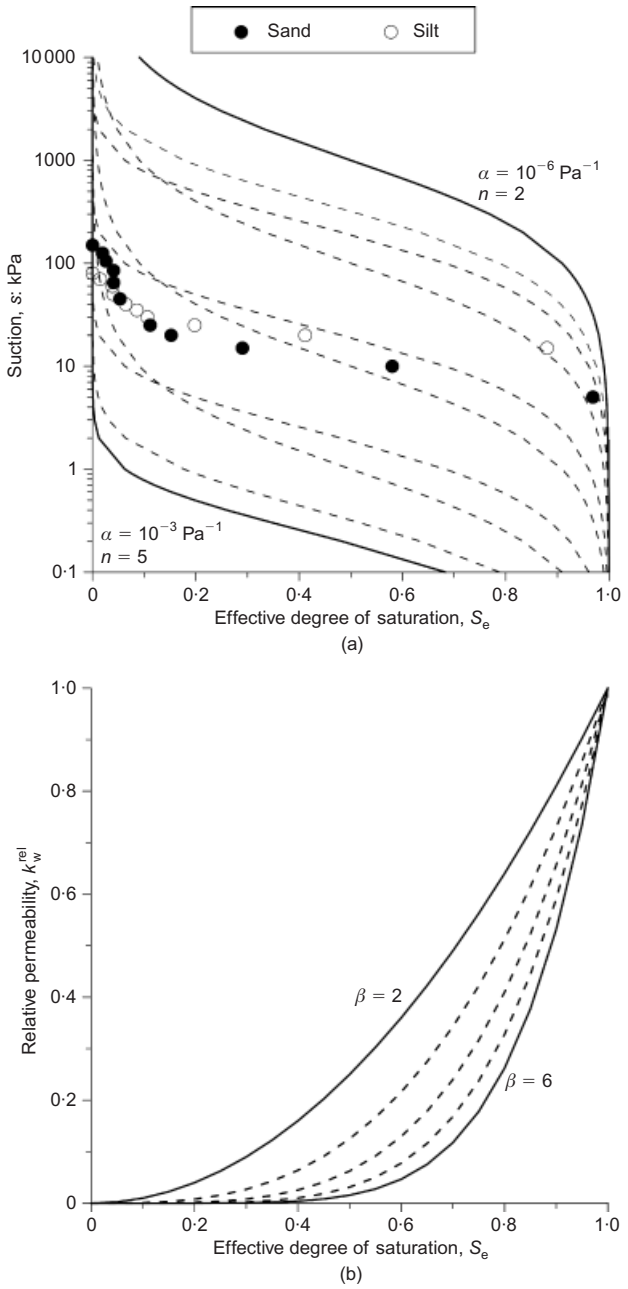


Fig. 12. Domain explored in terms of: (a) water retention curve; (b) relative permeability function. Continuous lines and points represent boundaries of explored space and independent axis-translation data respectively

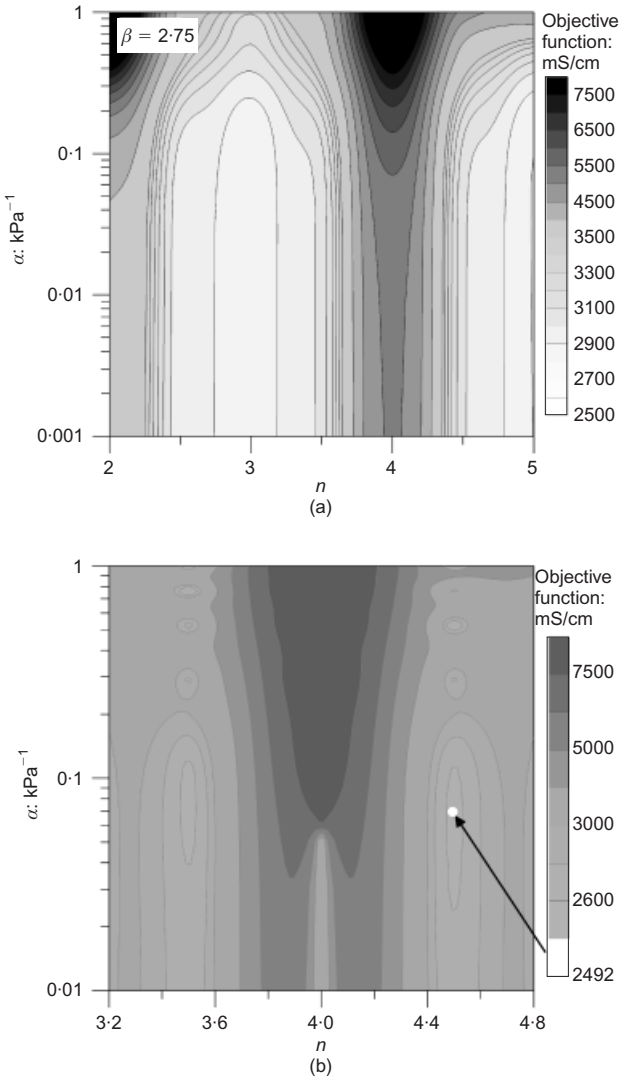


Fig. 13. Test 1A: (a) map of objective function $||e||_1$ for $\beta = 2{\cdot}75$ in n –log α space; (b) map of the objective function after refinement of grid. Section for $\beta = 2{\cdot}75$

are particular combinations of the minimum and maximum values of single parameters.

The inversion of Test 1A was based on tomographic reconstructions involving times $t_0 = 0$ (before drain opening) and $t_1 = 600$ s (after drain closure). An iso-error map, providing the values of the objective function for $\beta = 2$ in n –log α space, is given in Fig. 13(a). The choice of a logarithmic scale for α is due to the wide range of variation of this parameter. Several local minima are found: thus a solution method based on a local search approach (e.g. the Gauss–Newton method) is not applicable. The search grid in the parameter space was instead refined locally to identify the absolute minimum, whose position is given in Fig. 13(b).

The estimated best-fitting parameters are $\alpha = 7{\cdot}75 \times 10^{-2}$ kPa^{-1}, $n = 4{\cdot}5$ and $\beta = 2{\cdot}75$. Reconstructed and simulated electrical conductivities are reported in Fig. 14 ($t = 10$ min after drain closure). The estimated water retention curve, indicated with the continuous line, and the independent experimental data (wetting branch) are compared in Fig. 15. A satisfactory agreement is obtained, with a slight overestimation of the air entry value.

The same procedure was applied for Test 2A, which was performed on the sand specimen at a slow inflow rate. The solution of the inverse problem was based on tomographic reconstructions carried out during inflow at times $t_1 = 420$ s, $t_2 = 900$ s, $t_3 = 1380$ s, $t_4 = 1860$ s and $t_5 = 2340$ s. In this case, a regular pattern of iso-error maps was obtained, leading to a straightforward determination of the absolute minimum. The inverse problem was better constrained for the low inflow rate test (2A) than for the high inflow rate test (1A). The estimated parameters are $\alpha = 0{\cdot}1$ kPa^{-1}, $n = 2{\cdot}5$ and $\beta = 2$. A comparison of the retention curve estimated from Test 2A (dotted line) and the experimental data is reported in Fig. 15. Despite the difference in the iso-error maps of the two tests, the reconstructed curves do not differ significantly. The curve from Test 2A agrees more closely with the experimental data in the near-saturation and residual zones, while the slope is slightly overestimated at intermediate degrees of saturation.

Figure 16 shows the water retention curves as predicted from the inverse analysis of Tests 1B and 2B. Both predictions

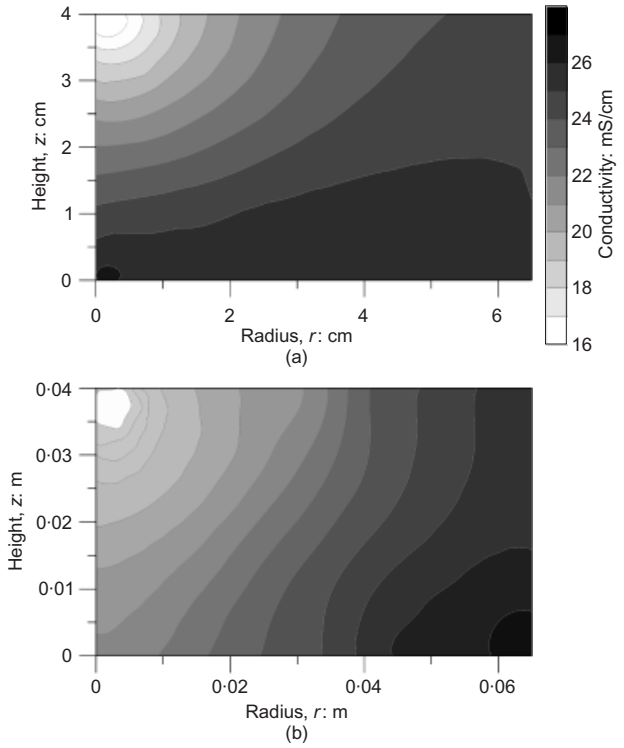


Fig. 14. Test 1A: comparison between (a) reconstructed and (b) simulated electrical conductivity distribution inside sample (values in mS/cm)

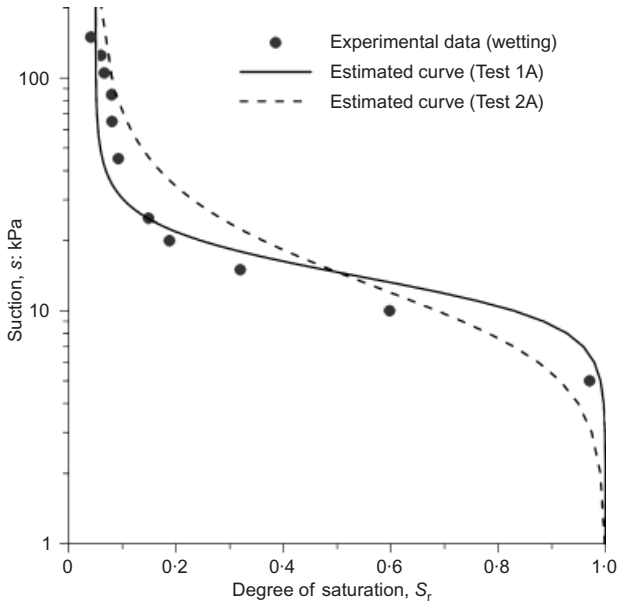


Fig. 15. Comparison between estimated retention curves for sand (Tests 1A and 2A) and independent experimental data obtained with axis-translation technique

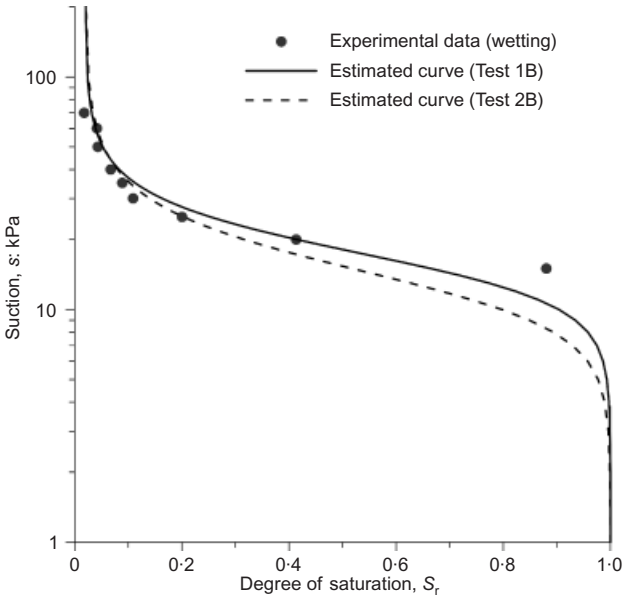


Fig. 16. Comparison between estimated retention curves for silt (Tests 1B and 2B) and independent experimental data obtained with axis-translation technique

agree with the experimental points determined independently with the axis-translation technique. The estimated parameters for the entire dataset are summarised in Table 4. The estimated values of the relative permeability exponent β exhibit variations around 3, which is the theoretical value for soils having uniform grain size and/or pore sizes (Bear, 1972).

SUMMARY AND CONCLUSIONS

In this work, electrical resistivity tomography (ERT) was used to monitor local water content changes during transient wetting processes in sand and silt laboratory samples.

Three-dimensional tomographic monitoring was then used to solve an inverse problem aimed at estimating the parameters of the water retention curve and of the relative permeability function. The water retention curves obtained from the inversion procedure are comparable with the reference curves obtained with the axis-translation technique.

The success of the quantitative interpretation relies on the agreement between the measured and reconstructed global masses of water. It was then assumed that this agreement also exists at the local scale. Thus the wetting and homogenisation processes occurring within the ERT oedometer, instead of being analysed as physical stages of a single volume element, were simulated by considering the processes as small-scale tests. Optimisation was then pursued based on a large number of local observations. To the authors' knowledge this is the first time that a comprehensive unsaturated hydraulic characterisation has been effectively achieved by interpreting ERT measurements with the above described approach.

Table 4. Estimated hydraulic parameters

Test ID	Material	α: kPa^{-1}	n	β
1A	Sand	$7{\cdot}75 \times 10^{-2}$	4·5	2·75
2A	Sand	$1{\cdot}00 \times 10^{-1}$	2·5	2
1B	Silt	$6{\cdot}32 \times 10^{-2}$	4	3
2B	Silt	$7{\cdot}75 \times 10^{-2}$	3·5	3

Moderate preliminary characterisation is needed, involving determination of the absolute hydraulic conductivity and of the relationship between electrical conductivity and degree of saturation. For this procedure, only electrical and hydraulic measurements are needed, and there is no need for other experimental tools, such as tensiometers or suction control devices. Given the typical difficulties arising in relative permeability measurement, and the considerable time needed to obtain water retention curves with other conventional techniques, the above-stated results encourage further research efforts in this field.

The proposed methodology could be used to investigate further some hydraulic features that are often neglected, such as the influence of applied stress, lateral confinement and previous hydro-mechanical history. This approach could also be adopted to estimate global hydraulic model parameters at the field scale, if detailed knowledge of the actual initial and boundary conditions is available.

ACKNOWLEDGEMENTS

This work was partially supported by the research project SoilCam funded by the EU Commission 7th FP (FP7-ENV-2007.3.1.2.2.) and by the National Research Project PRIN 2008B5T829_004. The authors wish to acknowledge Dr Francesco Cecinato for his help in improving the quality of the manuscript.

NOTATION

$\|\ldots\|_1$ L1 norm
B_w bulk compressibility of water
$\boldsymbol{e}$ prediction error, or misfit
e void ratio
k_a air conductivity
k_a^{dry} air conductivity in dry conditions
k_w hydraulic conductivity
k_w^{rel} relative permeability
k_w^{sat} hydraulic conductivity in saturated conditions
m, n parameters of the van Genuchten relationship for the water retention curve
m_a mass fraction of air
p exponent of porosity in Archie's law
q exponent of degree of saturation in Archie's law
$\boldsymbol{q}_a$ air specific discharge
$\boldsymbol{q}_w$ water specific discharge
R ideal gas constant
r radius of sample
S_e effective degree of saturation
S_r degree of saturation
$\overline{S}_r$ average degree of saturation of the sample, measured value
$\overline{S}_r^*$ average degree of saturation of the sample, reconstructed value
$\overline{S}_r^{RES}$ residual degree of saturation
s matric suction
T absolute temperature
t time
u_a air pressure
u_w water pressure
V_V volume of voids inside the sample
V_w volume of water inside the sample
α parameters of the van Genuchten relationship for the water retention curve
β exponent of the degree of saturation in the relationship defining the relative permeability
ρ_a mass density of air
ρ_w mass density of water
ρ_{w0} density of water at atmospheric pressure
σ electrical conductivity of the soil
$\boldsymbol{\sigma}$, $\boldsymbol{\sigma}^*$ vectors of nodal values of the simulated and reconstructed electrical conductivity
$\overline{\sigma}^*$ average value of the reconstructed electrical conductivity
σ_{sat} electrical conductivity of the soil in saturated conditions
σ_w electrical conductivity of the interstitial water
τ dummy time variable
ϕ porosity

REFERENCES

Archie, G. E. (1942). The electrical resistivity log as an aid to determining some reservoir characteristics. *Trans. AIME* **146**, 54–63.

Attia, A. M., Fratta, D. & Bassiouni, Z. (2008). Irreducible water saturation from capillary pressure and electrical resistivity measurements. *Oil Gas Sci. Technol*. **63**, No. 2, 203–217.

Battle-Aguilar, J., Schneider, S., Pessel, M., Tucholka, P., Coquet, Y. & Vachier, P. (2009). Axisymmetrical infiltration in soil imaged by non-invasive electrical resistivimetry. *Soil Sci. Soc. Am. J.* **73**, No. 2, 510–520.

Bear, J. (1972). *Dynamics of fluids in porous media*. New York: American Elsevier.

Binley, A., Cassiani, G., Middleton, R. & Winship, P. (2002). Vadose zone flow model parameterisation using cross-borehole radar and resistivity imaging. *J. Hydrol*. **267**, Nos 3–4, 147–159.

Blewett, J., McCarter, W. J., Chrisp, T. M. & Starrs, G. (2001). Monitoring sedimentation of a clay slurry. *Géotechnique* **51**, No. 8, 723–728, http://dx.doi.org/10.1680/geot.2001.51.8.723.

Blewett, J., McCarter, W. J., Chrisp, T. M. & Starrs, G. (2003). An experimental study on ionic migration through saturated kaolin. *Engng Geol*. **70**, Nos 3–4, 281–291.

Borsic, A., Comina, C., Foti, S., Lancellotta, R. & Musso, G. (2005). Imaging heterogeneities with electrical impedance tomography: laboratory results. *Géotechnique* **55**, No. 7, 539–547, http://dx.doi.org/10.1680/geot.2005.55.7.539.

Brooks, R. H. & Corey, A. J. (1964). *Hydraulic properties of porous media*, Hydrology Papers No. 3. Fort Collins, CO: Colorado State University.

Comina, C., Foti, S., Lancellotta, R., Musso, G. & Borsic, A. (2005). Imaging heterogeneities and diffusion in sand samples. *Proc. 11th Int. Conf. of Int. Assoc. of Computer Methods and Advances in Geomechanics, Torino* **2**, 27–34.

Comina, C., Foti, S., Musso, G. & Romero, E. (2008). EIT oedometer – an advanced cell to monitor spatial and time variability in soil. *Geotech. Test. J. ASTM* **31**, No. 5, 404–412.

Corey, A. T. (1954). The interrelations between gas and oil relative permeabilities. *Producers Monthly* **19**, 38–41.

Dalla, E., Cassiani, G., Brovelli, A. & Pitea, D. (2004). Electrical conductivity of unsaturated porous media: pore-scale model and comparison with laboratory data. *Geophys. Res. Lett*. **41**. doi: 10.1029/2003GL019170.

Damasceno, V. M., Fratta, D. & Bosscher, P. J. (2009). Development and validation of a low-cost electrical resistivity tomographer for soil process monitoring. *Can. Geotech. J.* **46**, No. 7, 842–854.

Deiana, R., Cassiani, G., Kemna, A., Villa, A., Bruno, V. & Bagliani, A. (2007). An experiment of non invasive characterization of the vadose zone via water injection and cross-hole time-lapse geophysical monitoring. *Near Surf. Geophys*. **5**, No. 3, 183–194.

Fredlund, D. G. & Rahardjo, H. (1993). *Soil mechanics for unsaturated soils*. New York: Wiley.

Hadamard, J. (1902). Sur les problèmes aux dérivées partielles et leur signification physique. *Princeton Univ. Bull* **13**, 49–52.

Hillel, A. C., Ferrè, T. P. A., Vrugt, J. A., Huisman, J. A., Moyses, S., Rings, S. & Kowalsky, M. B. (2010). Improved extraction of hydrologic information from geophysical data through coupled hydrogeophysical inversion. *Water Resour. Res*. **46**. doi: 10.1029/2008WR007060.

Hopmans, J. W. & Šimünek, J. (1999). Review of the inverse estimation of unsaturated hydraulic properties. *Proceedings of the international workshop on the characterization and measurement of the hydraulic properties of unsaturated porous media*, Riverside, CA, pp. 643–659.

Jinguuji, M., Toprak, S. & Kunimatsu, S. (2007). Visualization technique for liquefaction process in chamber experiments by using electrical resistivity monitoring. *Soil Dynam. Earthqu. Engng* **27**, No. 3, 191–199.

Kalinsky, R. J. & Kelly, W. E. (1993). Estimating water content of

soils from electrical resistivity. *Geotech. Test. J.* **16**, No. 3, 323–329.

Kemna, A., Vanderborght, J., Kulessa, B. & Vereecken, H. (2002). Imaging and characterisation of subsurface solute transport using electrical resistivity tomography (ERT) and equivalent transport models. *J. Hydrol*. **267**, Nos 3–4, 125–146.

Kool, J. B., Parker, J. C. & van Genuchten, M. T. (1987). Parameter estimation for unsaturated flow and transport models: a review. *J. Hydrol*. **91**, Nos 3–4, 255–293.

Kool, J. B. & Parker, J. C. (1988). Analysis of the inverse problem for transient unsaturated flow. *Water Resour. Res*. **24**, No. 6, 817–830.

Kuganenthira, N., Zhao, D. & Anandarajah, A. (1996). Measurement of fabric anisotropy in triaxial shearing. *Géotechnique* **46**, No. 4, 657–670, http://dx.doi.org/10.1680/geot.1996.46.4.657.

Lee, J. Y. & Santamarina, J. C. (2010). Electrical resistivity tomography in cylindrical cells: guidelines for hardware pre-design. *Geotech. Test. J.* **33**, No. 1. doi: 10.1520/GTJ102366.

Masrouri, F., Bicalho, K. V. & Kawai, K. (2008). Laboratory hydraulic testing in unsaturated soils. *Geotech. Geol. Engng* **26**, No. 6, 691–704.

McCarter, W. J. & Desmazes, P. (1997). Soil characterization using electrical measurements. *Géotechnique* **47**, No. 1, 179–183, http://dx.doi.org/10.1680/geot.1997.47.1.179.

McCarter, W. J., Blewett, J., Chrisp, T. M. & Starrs, G. (2005). Electrical property measurements using a modified hydraulic oedometer. *Can. Geotech. J.* **42**, No. 2, 655–662.

Menke, W. (1989). *Geophysical data analysis: Discrete inverse theory*. San Diego, CA: Academic Press.

Michot, D., Benderitter, Y., Dorigny, A., Nicoullaud, B., King, D. & Tabbagh, A. (2003). Spatial and temporal monitoring of soil water content with an irrigated corn crop cover using surface electrical resistivity tomography. *Water Resour. Res*. **39**, No. 5. doi: 10.1029/2002WR001581.

Mitchell, J. K. & Soga, K. (2005). *Fundamentals of soil behavior*. New York: Wiley.

Reynolds, J. M. (1997). *An introduction to applied environmental geophysics*. Chichester: Wiley.

Romano, N. & Santini, A. (1999). Determining soil hydraulic functions from evaporation experiments by a parameter estimation approach: experimental verifications and numerical studies. *Water Resour. Res*. **35**, No. 11, 3343–3359.

Romero, E., Lloret, A. & Gens, A. (1995). Development of a new suction and temperature controlled cell. *Proc. 1st Int. Conf. on Unsaturated Soils, Paris* **2**, 553–559.

Santamarina, J. C., with Klein, K. A. & Fam, M. A. (2001). *Soils and waves*. New York: Wiley.

Singha, K. & Gorelick, S. M. (2005). Saline tracer visualized with three-dimensional electrical resistivity tomography: field-scale spatial moment analysis. *Water Resour. Res*. **41**, W05023. doi: 10.1029/2004WR003460

Tikhonov, A. N. & Arsenin, V. Y. (1977). *Solutions of ill-posed problems*. New York: Winston.

Vanderborght, J., Kemna, A., Hardelauf, H. & Vereecken, H. (2005). Potential of electrical resistivity tomography to infer aquifer transport characteristics from tracer studies: a synthetic case study. *Water Resour. Res*. **41**, W06013. doi: 10.1029/2004WR003774.

van Genuchten, M. Th. (1980). A closed-form equation for predicting the hydraulic conductivity of unsaturated soils. *Soil Sci. Soc. Am. J.* **44**, No. 5, 892–898.

Young, M. H., Karagunduz, A., Šimůnek, J. & Pennell, K. D. (2002). A modified upward infiltration method for characterizing soil hydraulic properties. *Soil Sci. Soc. Am. J.* **66**, No. 1, 57–64.

Zhou, Q. Y., Shimada, J. & Sato, A. (2001). Three-dimensional spatial and temporal monitoring of soil water content using electrical resistivity tomography. *Water Resour. Res*. **37**, No. 2, 273–285.